frontiers | Frontiers in Earth Science

ORIGINAL RESEARCH
published: 20 June 2022
doi: 10.3389/feart.2022.798791

Stability Assessment of Multi-Stage Slopes Considering Local Failure

Haochen Wu[1], *Miaojun Sun*[2]* *and Jinnan Wang*[3]

[1]Zhejiang Provincial Seaport Investment & Operation Group Co., Ltd., Ningbo, China, [2]Powerchina Huadong Engineering Corporation Limited, Zhejiang Engineering Research Center of Marine Geotechnical Investigation Technology and Equipment, Hangzhou, China, [3]School of Civil Engineering and Architecture, Zhejiang Sci-Tech University, Hangzhou, China

The analytical method for slope stability analysis requires a collapse mechanism in advance. The collapse mechanism for a multi-staged slope is generally assumed to be overall failure, whereas this kind of slope may suffer from local failure. However, a local failure is rarely reported in the previous research for multi-staged slopes, which may result in an overestimate for slope stability. To this end, local failure is incorporated into the collapse mechanism for the first time, so as to develop a complete approach to assess the stability of multi-stage slopes. The modified pseudo-dynamic method is conducted to properly account for seismic effects. Thanks to the limit analysis method and strength reduction technique, the safety factor of a multi-stage slope is obtained. The result obtained by the presented approach shows a good agreement with that of previous literature and numerical calculations. The collapse mechanism of multi-stage slopes is studied, and the safety factor is presented schematically for a wide range of parameters. The results show that the local failure for a multi-stage slope often manifests under the intense seismic effects.

Keywords: multi-stage slope, overall failure, local failure, seismic effect, modified pseudo-dynamic approach

OPEN ACCESS

Edited by:
Yun JIA,
University in Lille, France

Reviewed by:
Zhibin Sun,
Hefei University of Technology, China
Nipa Chanda,
CMR Institute of Technology (CMR IT), India

***Correspondence:**
Miaojun Sun
sunmj816@hotmail.com

Specialty section:
This article was submitted to Structural Geology and Tectonics, a section of the journal Frontiers in Earth Science

Received: *20 October 2021*
Accepted: *26 April 2022*
Published: *20 June 2022*

Citation:
Wu H, Sun M and Wang J (2022) Stability Assessment of Multi-Stage Slopes Considering Local Failure. Front. Earth Sci. 10:798791. doi: 10.3389/feart.2022.798791

INTRODUCTION

Slope instability is one of the most concerned themes in geotechnical engineering, yet the stability assessment for multi-stage slopes is scarce. In fact, multi-stage slopes are widely found in nature and practical projects (Yang and Long, 2015; Yang and Li, 2018; Wang et al., 2020b). For this type of slope, it may be subjected to local instability apart from overall instability. However, previous studies have not drawn attention to local instability of multi-staged slopes, leading to overestimates of slope stability. Therefore, it is necessary to present a complete approach for assessing the stability of multi-stage slopes.

The current approaches for stability analysis of a slope consist of the limit equilibrium method (LEM) (Bishop, 1954; Morgenstern and Price, 1965; Zhou and Cheng, 2013), the limit analysis method (LAM) (Chen, 1975; Pan et al., 2017), and numerical simulation approaches, such as the finite element method (FEM) (Griffiths and Marquez, 2007), the discrete element method (DEM) (Wang et al., 2020), and the finite difference method (FDM) (Shen and Karakus, 2014). The particular advantage of the numerical simulation approach is that it could demonstrate the progressive nature of slope failure, without prescribing a specific collapse mechanism. While this approach possesses the special ability, it demands to provide many explicit geometrical and mechanical parameters. The LEM and LAM are based on the mechanics and kinematics underpinning respectively, considering the yield condition along the failure surface, whereas the collapse mechanisms of the two approaches need to be prescribed previously. Even so, compared to

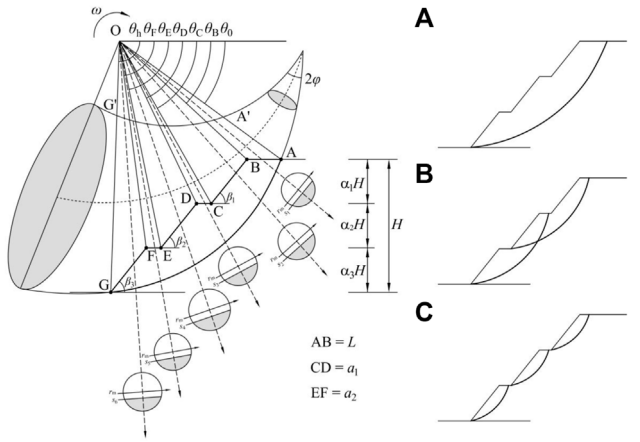

FIGURE 1 | Collapse mechanism of the multi-stage slope: **(A)** overall failure; **(B)** local failure of two stage; **(C)** local failure of single stage.

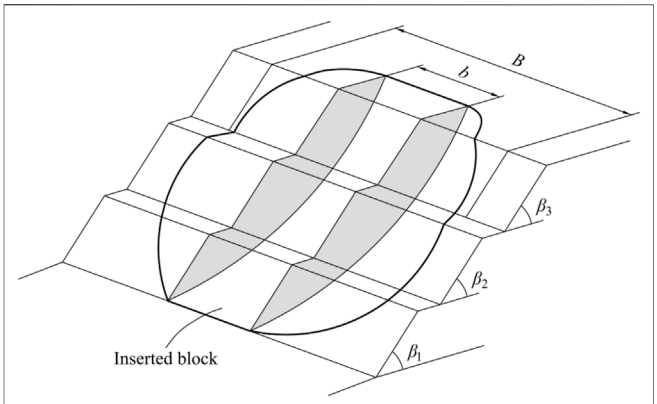

FIGURE 2 | Schematic diagram of the composite collapse mechanism for the multi-stage slope.

TABLE 1 | Comparison of the results with Michalowski and Drescher (2009) for $\varphi = 30°$

β	Results	B/H				
		1.0	2.0	3.0	5.0	10.0
45°	Michalowski and Drescher	54.850	42.732	39.956	37.994	36.703
	Present study	0.9967	0.9997	1.0004	1.0004	1.0004
60°	Michalowski and Drescher	23.835	19.103	17.873	17.063	16.527
	Present study	0.9924	0.9973	0.9997	1.0004	1.0004
75°	Michalowski and Drescher	14.701	12.109	11.184	10.628	10.265
	Present study	0.9985	0.9875	0.9973	0.9991	1.0004

the LEM which is an approximate approach, the LAM provides a rigorous upper bound solution (Chen, 1975; Michalowski, 2013) and widely applies to assess the slope stability and geotechnical engineering (Li and Yang, 2020; Zhang and Yang, 2021; Zhong and Yang, 2021). Recently, Michalowski and Drescher (2009) developed a novel three-dimensional (3D) collapse mechanism for slopes, which vastly promoted the LAM to solve the stability problems of 3D slopes. After that many scholars extended this collapse mechanism to the stability assessment for seismic displacements of slopes (Nadukuru and Michalowski, 2013), slopes reinforced piles (Gao et al., 2015), and slopes with cracks (He et al., 2019; Wang et al., 2019). However, the obtained conclusions of the previous literature are only suitable for single-stage slopes. More recently, Yang and Li (2018) calculated the safety factors of 3D two-stage slopes subjected to seismic effects and surcharges. Wang et al. (2019) compared the collapse mechanisms of different 3D compound slopes, and the slope stability was predicted by calculating the critical height. Man et al. (2020) assessed the probabilistic stability of a multi-stage slope but was limited to 2D cases. Although the multi-staged slopes have attracted a little attention, the collapse mechanisms of these researches are all assumed to be overall failure. For some special cases of multi-stage slopes, such as the multi-stage slope with a small slope angle in the lower stage but a large slope angle in the upper stage, local instability must be paid attention to. Apparently, the previous research about multi-stage slopes is still defective and incomplete. Local failure of multi-stage slopes should be incorporated into the collapse mechanism. Furthermore, the effects of external loads, soil parameters, and slope shapes (such as slope angles and aspect ratios) on the collapse mechanism and multi-stage slope stability should be further explicit.

For the cause of slope instability, the earthquake force is a significant external load that cannot be neglected (Terzaghi 1950; Baker et al., 2006; Chen et al., 2020). Over a long period of time, the pseudo-static method (PSM) was the mainstream to consider the seismic effect until the pseudo-dynamic method (PDM) was put forth (Steedman and Zeng, 1990). The PDM considers the spatiotemporal effects of seismic actions other than the PSM tackling the seismic force as a constant. (Steedman and Zeng, 1990). Subsequently, the PDM was applied to estimate the seismic active earth pressure for retaining walls by combining the LEM (Choudhury and Nimbalkar, 2006; Ghosh, 2008), which greatly promoted the development of PDM. In recent years, Qin and Chian (2018, 2019) have introduced the PDM into LAM to assess the slope stability in soil and rock media, whereas the 3D effects were not considered. The PSM simplify the dynamic load as inertia force, which neglects the inherent frequency and velocity of shear wave. To some extent, the PDM has offset these defects and made great progress in accounting for the seismic effect.

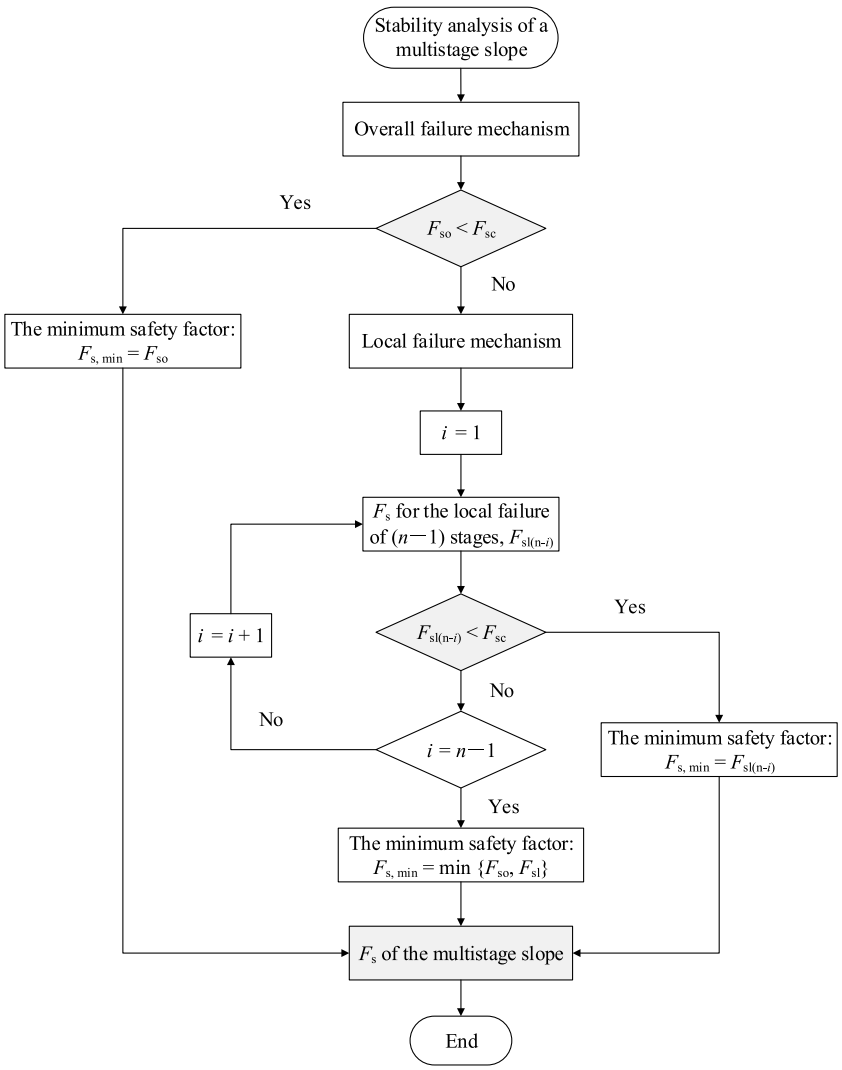

FIGURE 3 | Flow diagram of the stability analysis for multi-stage slopes.

However, the zero-stress boundary condition at the free surface is overlooked in the PDM (Choudhury and Katdare, 2013), and the damping effects of materials are not considered (Bellezza, 2015). To overcome the flaws of PDM, some corrections have been carried out, which further improved the rationality and accuracy of this approach (Pain et al., 2017; Qin and Chian, 2020). Here our goal is to apply the advanced modified PDM to the more challenging seismic stability problem of a multi-stage slope.

The present study aims to provide a complete approach to assess the stability of a multi-stage slope. For the first time, the 3D collapse mechanism put forward by Michalowski and Drescher (2009) for single-stage slopes is extended to consider both local failure and overall failure of multi-stage slopes. Thanks to the upper bound of LAM as well as the strength reduction technique, safety factors of multi-stage slopes can be extrapolated. Seismic effects are revisited by the application of the advanced modified PDM. The proposed approach is verified by degenerating multi-stage slopes into single-stage slopes and comparing the solutions with existing data. Finally, some illustrative examples and parametric analyses are applied to reveal the effects of slope shapes, soil parameters, and seismic effects on the collapse mechanism and the safety factor for a multistage slope. The main contribution of this study is that it performs a more complete approach for the stability analysis of a multi-stage slope.

MODIFIED PSEUDO-DYNAMIC APPROACH

According to Chen and Liu (1990), vertical seismic effects are significantly less vital when compared with horizontal seismic effects. Thus, only the horizontal effects are generally included in the stability analysis of slopes (Chen and Liu, 1990; Li et al., 2020b; Zhang and Yang, 2021). The previous PDM considers the soil as a linear elastic material, which results in an unrealistic infinite amplification of seismic waves (Bellezza, 2015). To this

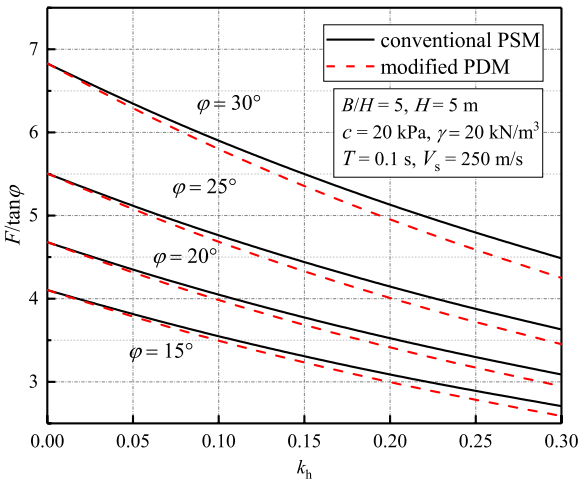

FIGURE 4 | Comparison of the results obtained by the PSM and the modified PDM. Corresponding parameters: $\alpha_1 = \alpha_2 = \alpha_3 = 1/3$, $\beta_1 = \beta_2 = \beta_3 = 45°$, $a_1 = a_2 = 0$. $\beta_1 = 45°$, $\beta_1 = 55°$, $\beta_1 = 65°$

TABLE 2 | Comparison of the results with Li et al. (2020b) for $k_h = 0.1$

c/γH tan φ	Results	B/H			
		2.0	3.0	5.0	∞
0.5	Li et al. (2020b)	4.50	4.54	4.42	4.30
	Present study	4.84	4.41	4.29	4.18
1.0	Li et al. (2020b)	8.30	7.43	7.18	6.95
	Present study	8.08	7.21	6.97	6.74
1.5	Li et al. (2020b)	11.54	10.24	9.86	9.51
	Present study	11.23	9.94	9.56	9.21
2.0	Li et al. (2020b)	14.76	13.02	12.50	12.03
	Present study	14.37	12.64	12.12	11.65

end, the assumption of a more realistic visco-elastic material is introduced here to modify the previous method. Moreover, the damping properties of the soil and the free-surface boundary condition are also considered. Soils are regarded as the Kelvin-Voigt medium which consists of a purely elastic spring and a purely viscous dashpot in parallel, so as to respect the viscoelastic wave propagation (Kramer 1996). The shear strength of the Kelvin-Voigt medium is expressed as:

$$\tau = \gamma_s G + \eta \frac{\partial \gamma_s}{\partial t} \tag{1}$$

where γ_s and G represent the shear strain and shear modulus, respectively. η is the soil viscosity, which can be calculated by $\eta = 2G\mu/\omega$, where μ is the damping ratio of soils.

The motion equation of shear waves propagating vertically is expressed as:

$$\rho \frac{\partial u_h}{\partial t^2} = \frac{\partial \tau}{\partial z} \tag{2}$$

where ρ and u_h represent the soil density and horizontal displacement, respectively. z is the vertical distance to slope toe.

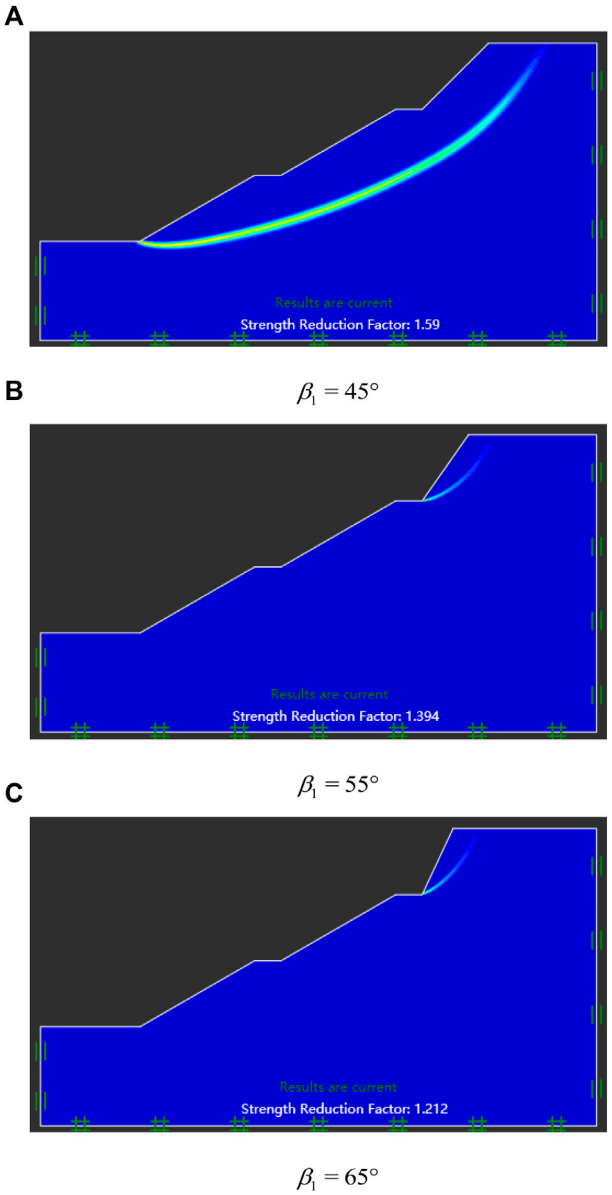

FIGURE 5 | Results of multi-stage slopes obtained by the FEM for LA. Corresponding parameters: $c = 20$ kPa, $\varphi = 28°$, $\gamma = 17.85$ kN/m^3, $H = 30$ m, $a_1 = a_2 = 4$ m, $\alpha_1 = \alpha_2 = \alpha_3 = 1/3$, $\beta_1 = \beta_2 = 30°$. **(A)** $\beta 3 = 45°$, **(B)** $\beta 3 = 55°$, **(C)** $\beta 3 = 65°$.

According to **Eqs 1**, **2**, the following differential equation can be obtained:

$$\rho \frac{\partial^2 u_h}{\partial t^2} = G \frac{\partial^2 u_h}{\partial z^2} + \eta \frac{\partial^3 u_h}{\partial z^2 \partial t} \tag{3}$$

By incorporating the boundary condition into the differential equation, the expression of u_h can be obtained. Two constraints are introduced: 1) zero stress condition at the slope crest ($z = H$); 2) horizontal displacement $u_{ht} = u_{h0}\cos(\bar{\omega}t)$ at the slope toe ($z = 0$). The expression of u_h is derived as:

TABLE 3 | Safety factors of all collapse mechanisms for multi-stage slopes.

β_1	Overall failure	local failure	local failure	local failure	local failure	local failure
	All stages	Two-stages	Two-stages	one stage	one stage	one stage
	Total	Upper	Lower	Upper	Middle	Lower
45°	1.591	1.645	1.952	1.620	2.160	2.160
55°	1.552	1.567	1.952	1.385	2.160	2.160
65°	1.523	1.510	1.952	1.194	2.160	2.160

Corresponding parameters: c = 20 kPa, φ = 28°, γ = 17.85 kN/m^3, H = 30 m, $a_1 = a_2$ = 4 m, $\alpha_1 = \alpha_2 = \alpha_3$ = 1/3, $\beta_1 = \beta_2$ = 30°.

TABLE 4 | Safety factors and collapse mechanisms of multi-stage slopes obtained by the present study.

β_1	Safety factor	Collapse mechanism
45°	1.591	overall failure- all stages- total
55°	1.385	local failure- one stage- upper
65°	1.194	local failure- one stage- upper

Corresponding parameters: c = 20 kPa, φ = 28°, γ = 17.85 kN/m^3, H = 30 m, B/H = 1000, $a_1 = a_2$ = 4 m, $\alpha_1 = \alpha_2 = \alpha_3$ = 1/3, $\beta_1 = \beta_2$ = 30°.

TABLE 5 | Safety factors and collapse mechanisms of multi-stage slopes under different seismic coefficients k_h.

kh	Safety factor	Collapse mechanism
0	1.591	overall failure- all stages- total
0.15	1.270	overall failure- all stages- total
0.3	1.057	local failure- one stage- lower

Corresponding parameters: c = 20 kPa, φ = 28°, γ = 17.85 kN/m^3, H = 30 m, B/H = 1000, $a_1 = a_2$ = 4 m, $\alpha_1 = \alpha_2 = \alpha_3$ = 1/3, β_1 = 45°, $\beta_1 = \beta_2$ = 30°.

$$u_h(z,t) = \frac{u_{h0}}{C_s^2 + S_s^2}\left[(C_{s1}C_{s2} + S_{s1}S_{s2})\cos(\bar{\omega}t) + (S_{s1}C_{s2} - C_{s1}S_{s2})\sin(\bar{\omega}t)\right] \quad (4)$$

where

$$C_{s1} = \cosh(z_{s2})\cos(z_{s1}) \quad (5)$$

$$S_{s1} = -\sinh(z_{s2})\sin(z_{s1}) \quad (6)$$

$$C_{s2} = \cos\left[z_{s1}\left(1 - \frac{z_i}{H}\right)\right]\cosh\left[z_{s2}\left(1 - \frac{z_i}{H}\right)\right] \quad (7)$$

$$S_{s2} = -\sin\left[z_{s1}\left(1 - \frac{z_i}{H}\right)\right]\sinh\left[z_{s2}\left(1 - \frac{z_i}{H}\right)\right] \quad (8)$$

$$z_{s1} = \frac{\bar{\omega}H}{V_s}\left[\frac{\sqrt{1+4\xi^2}+1}{2\left(1+4\xi^2\right)}\right]^{0.5} \quad (9)$$

$$z_{s2} = -\frac{\bar{\omega}H}{V_s}\left[\frac{\sqrt{1+4\xi^2}-1}{2\left(1+4\xi^2\right)}\right]^{0.5} \quad (10)$$

Thereupon the expression of a_h can be easily derived by differentiating u_h twice pertaining to t:

$$a_h(z,t) = \frac{k_h g}{C_{s1}^2 + S_{s1}^2}\left[(C_{s1}C_{s2} + S_{s1}S_{s2})\cos(\bar{\omega}t) + (S_{s1}C_{s2} - C_{s1}S_{s2})\sin(\bar{\omega}t)\right] \quad (11)$$

TABLE 6 | Safety factors and collapse mechanisms of multi-stage slopes under different ratios of B/H.

B/H	Safety factor	Collapse mechanism
1	1.726	local failure- one stage- upper
2	1.669	local failure- one stage- upper
3	1.652	local failure- one stage- upper
5	1.632	overall failure- all stages- total
10	1.611	overall failure- all stages- total
1,000	1.591	overall failure- all stages- total

Corresponding parameters: c = 20 kPa, φ = 28°, γ = 17.85 kN/m^3, H = 30 m, $a_1 = a_2$ = 4 m, $\alpha_1 = \alpha_2 = \alpha_3$ = 1/3, β_1 = 45°, $\beta_1 = \beta_2$ = 30°, k_h = 0.

TABLE 7 | Safety factors and collapse mechanisms of multi-stage slopes under different ratios of α_3.

α_3	Safety factor	Collapse mechanism
0.1	0.992	overall failure- all stages- total
0.2	1.040	overall failure- all stages- total
0.3	1.485	overall failure- all stages- total
0.4	1.366	overall failure- all stages- total
0.5	1.233	overall failure- all stages- total

Corresponding parameters: c = 20 kPa, φ = 28°, γ = 17.85 kN/m^3, H = 30 m, $a_1 = a_2$ = 4 m, B/H = 10, $\alpha_1 = \alpha_2 = (1 - \alpha_3)/2$, β_1 = 45°, $\beta_1 = \beta_2$ = 30°, k_h = 0.

Thereinto, $k_h g = -\bar{\omega}^2 u_{h0}$ and $\bar{\omega} = 2\pi/T$ are explicit. k_h is the seismic acceleration coefficient at the base, $\bar{\omega}$ is the angular velocity, and T represents the vibration period.

THREE-DIMENSIONAL COLLAPSE MECHANISM OF MULTI-STAGE SLOPES

The conventional plan-strain collapse mechanism provides a conservative estimation for slope stability. To this end, a 3D horn-like collapse mechanism was proposed and applied to slope stability (Michalowski and Drescher, 2009). Hereon, we extend this collapse mechanism to the multi-stage slope, as shown in **Figure 1**. The shape of the collapse mechanism is a curvilinear cone with an apex angle 2φ, ensuring the collapse mechanism complies with the associated flow law. The curvilinear cone, equipped with rounded radial cross-sections with varying diameters, rotates about an axis passing through point O. The boundary of the collapse mechanism is constrained by the upper

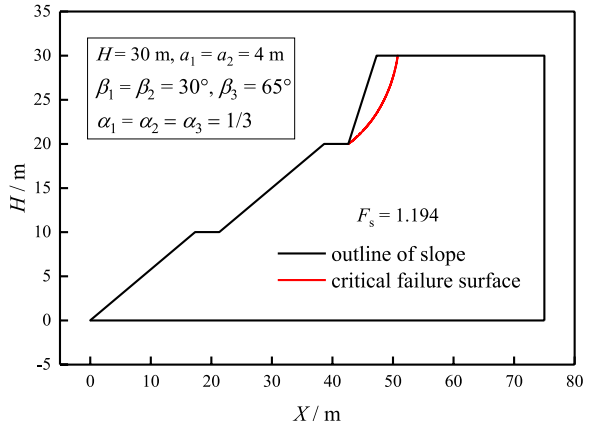

FIGURE 6 | Slip surface obtained by the present study. Corresponding parameters are the same as those in **Figure 5C**.

and lower log spirals. In the symmetry plane, the two constraints are expressed as, $A'G'$

$$r' = r'_0 e^{-(\theta-\theta_0)\tan\varphi} \tag{12}$$

and AG

$$r = r_0 e^{(\theta-\theta_0)\tan\varphi} \tag{13}$$

where r_0 = OA and $r_0' = OA'$ are shown in **Figure 1**, φ is the internal friction angle, and θ represents the included angle between the radius of log-spiral and the horizontal line.

The radius of the radial cross-section, R, and the distance from the center of cross-sections to point O, r_m, are defined as:

$$R = \left(r - r'\right)/2 = r_0 f_1 \tag{14}$$

$$r_m = \left(r - r'\right)/2 = r_0 f_2 \tag{15}$$

where the dimensionless expressions, f_1 and f_2, are attached in **Supplementary Appendix SA**.

Unlike single-stage slopes, the collapse mechanisms of multi-stage slopes include overall failure and local failure. **Figure 1A** shows the slip surface of overall failure in the symmetry plane. **Figure 1B** shows the two-stages slip surface of local failure, and **Figure 1C** shows the single-stage slip surface of local failure in the symmetry plane.

By splitting the 3D collapse mechanism through the symmetry plane and inserting a plane-strain failure block with the width b, a composite collapse mechanism can be obtained, as depicted in **Figure 2**. B represents the overall width of the collapse mechanism. The composite mechanism allows transition to a plane-strain one as the width of insert block $b \to \infty$. β_1, β_2, and β_3 represent the slope angle of each stage, respectively. α_1, α_2, and α_3 are depth coefficients that satisfy the following constraint:

$$\alpha_1 + \alpha_2 + \alpha_3 = 1 \tag{16}$$

In addition, some significant derivations of geometrical relations which has shown in **Figure 1** are provided in **Supplementary Appendix SA**. The variables in **Figure 1** corresponds to the same derivations in **Supplementary Appendix SA**

The upper bound of LAM requires establishing the work rate balance equation. Soil weights of the failure block and seismic actions contribute to the external work rates, namely W_γ and W_s respectively. The internal energy dissipation rates with regard to the soil resistance are denoted as D. Therefore, the balance equation for work rates is expressed as:

$$W_\gamma + W_s = D_c \tag{17}$$

The work rate W_γ is calculated by:

$$W_\gamma = \int_V \gamma v \cos\theta \mathrm{d}V = W_{\gamma-3D} + W_{\gamma-insert} \tag{18}$$

where γ refers to the soil unit weight, v represents the velocity of a mass point, and V is the volume of soil mass being shear failure. $W_{\gamma-3D}$ and $W_{\gamma-insert}$ represent the work rates of the 3D portion and the inserted portion, which are derived in **Supplementary Appendix SB**.

The work rates W_s can be obtained by:

$$W_s = \int_V \frac{\gamma}{g} a_h v_h \mathrm{d}V \tag{19}$$

where g is the acceleration of gravity, a_h represents the horizontal seismic acceleration, and v_h represents the horizontal velocity of the mass point.

The modified PDM considers the spatiotemporal effects of seismic waves, indicating that the seismic acceleration a_h is no longer constant, but varies with time and position. The present study introduces the layer-wise summation approach to calculate the work rates W_s, the detailed derivations of which are attached in **Supplementary Appendix SB**.

The internal energy dissipation D_c can be calculated by:

TABLE 8 | Safety factors and collapse mechanisms of multi-stage slopes under different widths of a_1 and a_2.

a_1	Safety factor	Collapse mechanism	a_2	Safety factor	Collapse mechanism
0	1.480	local failure- two-stages- upper	0	1.499	overall failure- all stages- total
1	1.524	local failure- two-stages- upper	1	1.526	overall failure- all stages- total
2	1.561	overall failure- all stages- total	2	1.553	overall failure- all stages- total
3	1.586	overall failure- all stages- total	3	1.581	overall failure- all stages- total
4	1.611	overall failure- all stages- total	4	1.611	overall failure- all stages- total
5	1.629	local failure- one stage- upper	5	1.629	local failure- one stage- upper

Corresponding parameters: c = 20 kPa, φ = 28°, γ = 17.85 kN/m^3, H = 30 m, B/H = 10, $\alpha_1 = \alpha_2 = \alpha_3$ = 1/3, β_1 = 45°, $\beta_1 = \beta_2$ = 30°, k_h = 0.

TABLE 9 | Safety factors and collapse mechanisms of multi-stage slopes under different soil parameters.

c	Safety factor	Collapse mechanism	φ	Safety factor	Collapse mechanism
15	1.421	local failure- one stage- upper	15	1.000	overall failure- all stages- total
20	1.611	overall failure- all stages- total	20	1.227	overall failure- all stages- total
25	1.713	overall failure- all stages- total	25	1.464	overall failure- all stages- total
30	1.806	overall failure- all stages- total	30	1.698	local failure- one stage- upper

Corresponding parameters: $\gamma = 17.85\,kN/m^3$, $H = 30\,m$, $B/H = 10$, $\alpha_1 = \alpha_2 = \alpha_3 = 1/3$, $a_1 = a_2 = 4$ m, $\beta_1 = 45°$, $\beta_1 = \beta_2 = 30°$, $k_h = 0$

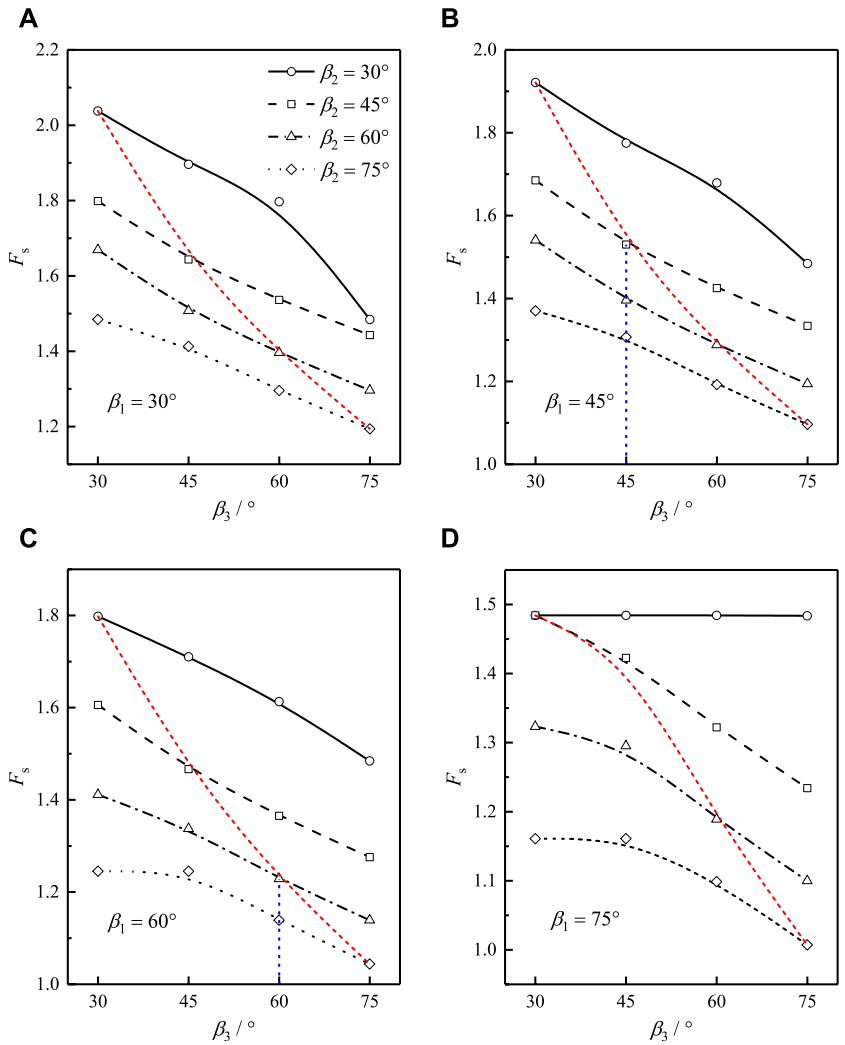

FIGURE 7 | Safety factors of multi-stage slopes with different slop angles: **(A)**$\beta_1 = 30°$; **(B)** $\beta_1 = 45°$; **(C)** $\beta_1 = 60°$; **(D)** $\beta_1 = 75°$. Corresponding parameters: $\alpha_1 = \alpha_2 = \alpha_3 = 1/3$, $a_1 = a_2 = 2$ m, $B/H = 2$, $k_h = 0$.

$$D_c = \int_S vc\cos\varphi dS = D_{3D} + D_{insert} \tag{20}$$

where c is cohesion, and S is the area of the slip surface. Similarly, D_{3D} and D_{insert} represent the energy dissipation rates in the 3D portion and inserted portion, respectively, which are given in **Supplementary Appendix SB**.

STABILITY ANALYSIS PROCESS OF MULTI-STAGE SLOPES

Safety Factor

The strength reduction technique is introduced to the upper bound of LAM to obtain the safety factor of multistage slopes, which is defined as follows:

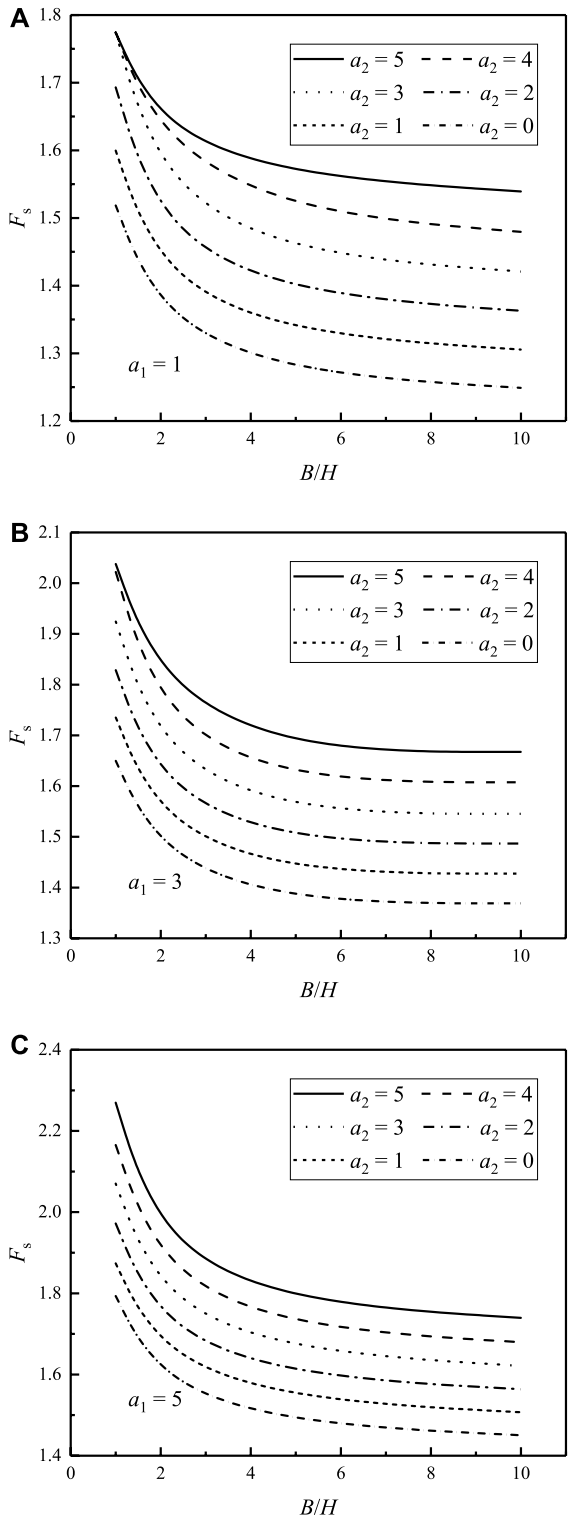

FIGURE 8 | Safety factors of multi-stage slopes with different step widths: **(A)** $a_1 = 1$; **(B)** $a_1 = 3$; **(C)** $a_1 = 5$. Corresponding parameters: $\alpha_1 = \alpha_2 = \alpha_3 = 1/3$, $\beta_1 = \beta_2 = \beta_3 = 45°$, $k_h = 0$.

$$F_s = \frac{\tan\varphi}{\tan\varphi'} = \frac{c}{c'} \tag{21}$$

where c' and φ' represent strength parameters under the critical state, F_s represents the safety factor.

It should be noted that the obtained calculations of safety factors are the upper bounds to the actual solutions. An optimization procedure is established to find out the minimum safety factor among all possible calculations. The best estimation of safety factors could be obtained by varying the variables: $\theta_0, \theta_h, r'/r_0, t$. To guarantee the collapse mechanism being valid, the assignment of these variates should satisfy the constraint conditions as follows:

$$\begin{cases} 0 < \theta_0 < \theta_B < \theta_C \le \theta_D < \theta_E \le \theta_F < \theta_h < \pi \\ 0 < r'/r_0 < 1 \\ 0 < \alpha_i < 1 \\ 0 \le t < T \end{cases} \tag{22}$$

Analytical Process of the Multi-Stage Slope

For most multi-stage slopes, it is much more possible to occur overall failure. However, for the multi-stage slopes with some special cases, the collapse mechanism not only includes overall failure but also local failure. If the mechanism of these types of slopes is assumed to be overall failure, it may result in incorrect estimation of slope stability.

The present study proposed a new analytical process for the stability assessment of multi-stage slopes. Firstly, it is required to define a critical safety factor F_{sc}, which may be referred to the design specification or the design requirement of specific engineering. Secondly, the safety factor of the overall collapse mechanism, F_{so}, should be compared with F_{sc}. Next, we need to make a comparison. If $F_{so} < F_{sc}$, it means that the multi-stage slope will explicitly be instability. Otherwise, it should determine whether local failure will occur. The safety factor of the local collapse mechanism is set as F_{sli}, where i represents the i th stage of the slope, and the total stages of the slope are n. If local failure occurs on the $(n-1)$ -stages of a multi-stage slope, local failure of the next stage [eg., $(n-2)$] is not considered, and so on until the minimum safety factor is obtained. The entire flow diagram of this analytical process is shown in **Figure 3**. Specifically, we take the advantage of an exhaustive method-based algorithm to obtain an initial feasible point, and a globally optimal solution is acquired by using the sequential quadratic program. In the optimization process, the constraint conditions in **Eq. 22** should be respected.

RESULTS AND DISCUSSION

Comparison

To verify the proposed approach for multi-stage slopes, three steps are carried out here to provide cogent comparisons. First, multi-stage slopes can be degraded into single-stage slopes in the case of $\beta_1 = \beta_2 = \beta_3$ and $a_1 = a_2 = 0$, and then the results

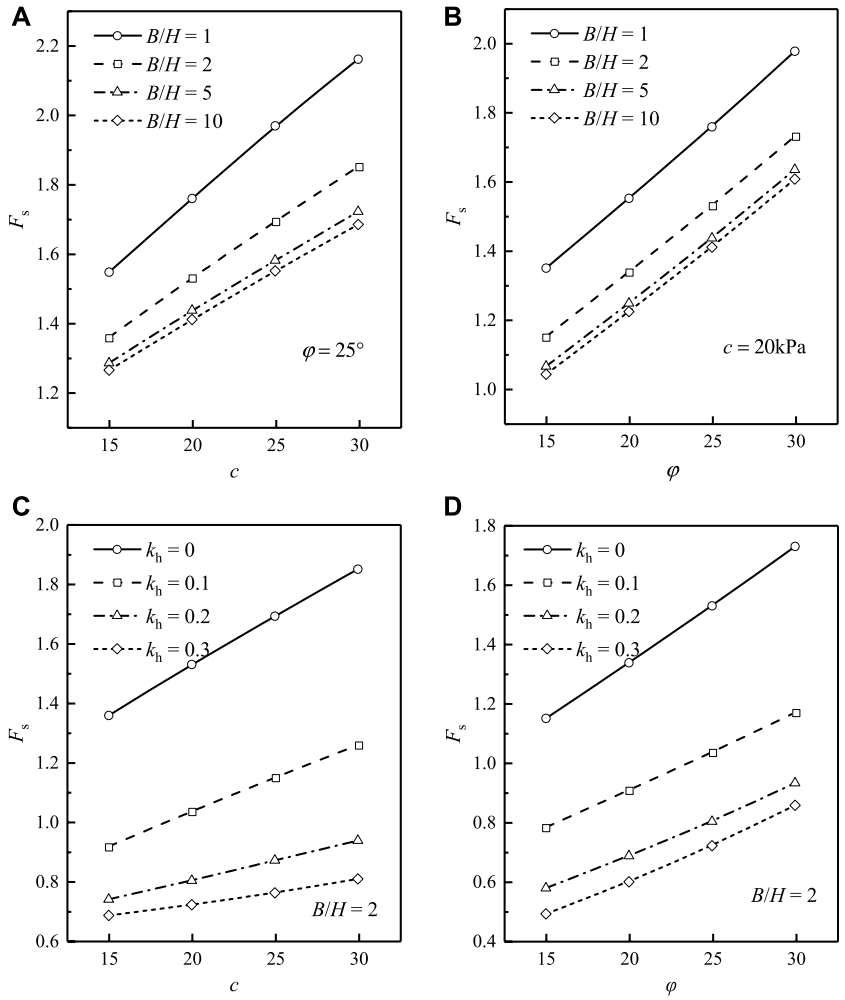

FIGURE 9 | Safety factors of multi-stage slopes with different soil parameters: **(A)** c, $k_h = 0$; **(B)** φ, $k_h = 0$; **(C)** c, $k_h = 0.1$; **(D)** φ, $k_h = 0.1$. Corresponding parameters: $\alpha_1 = \alpha_2 = \alpha_3 = 1/3$, $\beta_1 = \beta_2 = \beta_3 = 45°$.

obtained by the presented approach are compared to the solutions of Michalowski and Drescher (2009). Michalowski and Drescher (2009) provided the results of the critical height $\gamma H/c$, which represents the critical state of failure. Under the evaluation system of safety factors, the critical state of failure means the safety factor is equal to 1.0. As shown in **Table 1**, the calculated safety factors of the present study are highly closing to 1.0. Then, the seismic stability of single-stage slopes is estimated by the conventional PSM and the modified PDM respectively, as shown in **Figure 4**. The discrepancy of the results obtained from the two methods is small under the same conditions. In addition, the results of this study are compared with that of Li et al. (2020b), which provides the safety factors of 3D slopes subjected to pseudo-static seismic effects. As shown in **Table 2**, the results of the two studies show excellent agreement. Finally, three illustrative examples for multi-stage slopes are employed to verify the present approach. For comparison, the safety factors of multi-stage slopes are calculated by the FEM for LA in Optum G2, as illustrated in **Figure 5**. Meanwhile, **Table 3** provides the safety factors of all the collapse mechanisms for multi-stage slopes, and **Table 4** provides the final results of safety factors and the collapse mechanism for multi-stage slopes. In addition, **Figure 6** illustrates the slip surface obtained by the present study for the same multi-stage slope in **Figure 5C**. As expected, the results shown in **Table 4** and **Figure 6** coincide well with that of **Figure 5**, indicating the validity of the proposed approach.

Illustrative Example

In this section, the effects of different factors on the collapse mechanism for multi-stage slopes will be discussed by several illustrative examples. Firstly, the effect of seismic action is investigated, as shown in **Table 5**. We can conclude that safety factors of multi-stage slopes are getting smaller with the increase of k_h. Meanwhile, the collapse mechanism converts from overall failure to local failure. Secondly, **Table 6** provides the results with different aspect ratios of B/H. Multi-stage slopes suffer from local failure of one stage with $B/H < 3.0$, whereas overall failure occurs as B/H exceeds 3.0. For B/H exceeding 10.0, the safety factor and

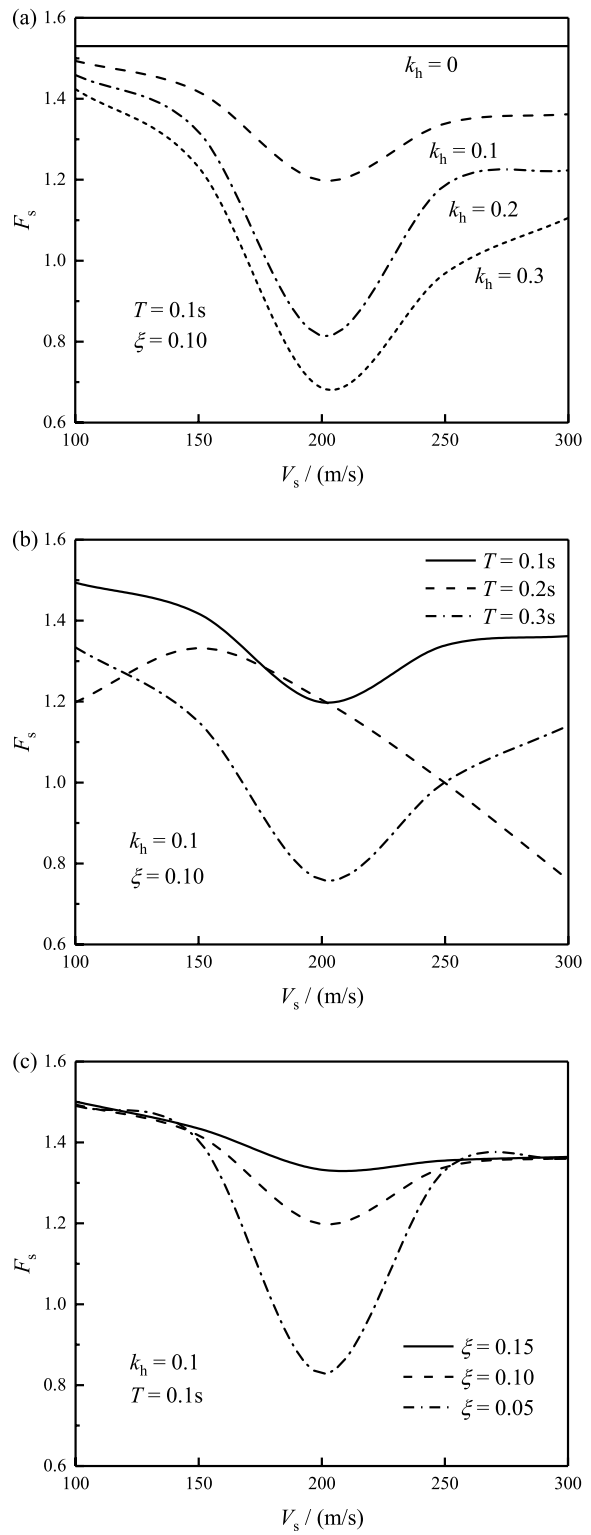

FIGURE 10 | Safety factors of multi-stage slopes with different shear wave velocities: **(A)** k_h; **(B)** T; **(C)** ξ. Corresponding parameters: $\alpha_1 = \alpha_2 = \alpha_3 = 1/3$, $a_1 = a_2 = 2$ m, $B/H = 2$, $\beta_1 = \beta_2 = \beta_3 = 45°$.

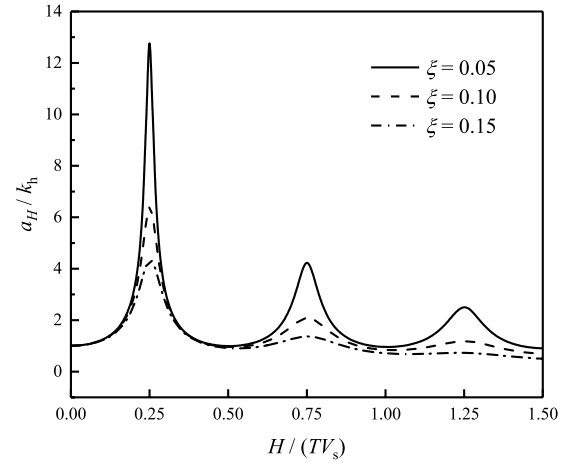

FIGURE 11 | Ratios of the acceleration amplitude at the surface to the base.

the collapse mechanism of multi-stage slopes have no significant changes. Next, to estimate the effects of depth coefficients, α_3 is taken as a variable, and α_1, α_2 is calculated by $\alpha_1 = \alpha_2 = (1 - \alpha_3)/2$. The results given in **Table 7** show that depth coefficients have no influence on the collapse mechanism of multi-stage slopes, but affect the safety factor. Finally, we focus on the effect of step width a_1, a_2. As shown in **Table 8**, the multi-stage slope undergoes local failure of two stages, overall failure, and local failure of one stage as the upper step width a_1 increases. Similarly, overall failure turns into local failure of one stage when the step width a_2 exceeds 4 m. The results in **Table 9** show that the soil parameters, c and φ, would affect the collapse mechanism of multi-stage slopes. The multi-stage slope with a small c or a large φ is more likely to suffer from local failure. In addition, a conclusion also can be obtained that the slope angle affects the collapse mechanism, as presented in **Table 4** and **Figure 6**.

In summary, we can conclude that seismic effects, ratios of B/H, step widths, and the slope angle have an apparent effect on the collapse mechanism of multi-stage slopes, indicating that considering local failure is much more reasonable for multi-stage slopes.

Parametric Analysis

This section is dedicated to analyzing the effects of seismic effects, soil parameters, and slope shapes on the stability of multi-stage slopes for a wide range of parameters. In the following discussion, soil parameters are assigned as: $H = 15$ m, $c = 20$ kPa, $\varphi = 25°$, $\gamma = 20$ kN/m^3. **Figure 7** provides safety factors of multi-stage slopes under different slope angles. It can be observed that safety factors of multi-stage slopes reduce apparently as slope angles increase at each stage. The red dash curve represents safety factors for multi-stage slopes with $\beta_2 = \beta_3$, the upper area of the red curve represents $\beta_2 < \beta_3$, and the lower area means $\beta_2 > \beta_3$. In addition, the blue dash curve in **Figure 7** is a dividing line, on the left of which represents $\beta_3 < \beta_1$ as well as $\beta_3 > \beta_1$ on the right. We can

observe that the multi-stage slope with $\beta_1 = 60°$, $\beta_2 = 75°$, $\beta_3 = 30°$, 45° in **Figure 7C**, $\beta_1 = 75°$, $\beta_2 = 30°$, $\beta_3 = 30°\sim75°$ in **Figure 7D**, and $\beta_1 = 75°$, $\beta_2 = 75°$, $\beta_3 = 30°$, 45° in **Figure 7D** are all subjected to local failure. Thus, we can conclude that the multi-stage slope with a smaller slope angle in the lower stage and a larger slope angle in the upper stage is more possibly subject to local failure. In other words, the areas on the left of the blue dash curve and below the red dash curve for multi-stage slopes are more possibly subject to local failure.

As illustrated in **Figure 8**, slope stability increases as the step width (a_1, a_2) increases. The points of intersection in **Figure 8A** and **Figure 8B** indicate that local failure occurs with a small aspect ratio, $B/H = 1$. So, it can be concluded that a large step width would improve the stability of a multi-stage slope, and the small ratio of B/H may result in local failure of a multi-stage slope. The results in **Figure 9A** and **Figure 9B** show that soil parameters significantly affect the safety factor, which increases linearly with the increase of c and φ. The results in **Figure 9C** and **Figure 9D** compared the safety factors of slopes with different seismic coefficients. It can be observed that the safety factors dramatically reduce with the increase of earthquake magnitude.

Figure 10 shows the variation of safety factors for different seismic parameters. It can be observed that the increase of acceleration coefficient k_h and the decline of damping ratio ξ prominently reduce the slope stability, whereas the variation of the shear wave velocity V_s leads to an apparent nonlinear trend on slope stability, especially with different values of vibration period T. To further scrutinize these variability trends, natural frequencies of soils lying over a rigid stratum and suffering from a shear wave (Kramer, 1996), which is denoted as:

$$\frac{\omega_n H}{V_s} = \frac{\pi}{2} + n\pi,\ n = 0,\ 1,\ 2..... \tag{23}$$

Submitting $\omega_n = 2\pi/T$, **Eq. 23** can be simplified as

$$\frac{H}{TV_s} = \frac{1}{4} + \frac{n}{2},\ n = 0, 1, 2 \ldots\ldots \tag{24}$$

Combining **Eq 24**, **11**, the ratio of the acceleration amplitude at the surface can be obtained, as shown in **Figure 11**. From **Figure 11**, we can find that the seismic acceleration amplitude is magnified as the frequency of seismic waves being close to the natural frequencies of soils. Moreover, a large damping ratio would decline the seismic acceleration amplitude. Thus, the vibration of seismic acceleration results in the variability trends of safety factors in **Figure 10**.

CONCLUSION

The 3D collapse mechanism for single-stage slopes is extended to consider local failure for multi-stage slopes. The modified PDM is introduced to properly depict the seismic effect. The influence of slope shapes, soil parameters, and seismic effects on the collapse mechanism as well as safety factors are investigated by some illustrative examples and parametric analyses. The following conclusions can be obtained:

1) For a multi-stage slope, the seismic effect, ratios of B/H, step widths, and the slope angle of each stage all have effects on the collapse mechanism and safety factors. The multi-stage slope with a smaller slope angle in the lower stage and a larger slope angle in the upper stage is more possibly subject to local failure. The slope with a large step width is more stable than that with a small one, and a small aspect ratio B/H or cohesion c may result in local failure. It is indicated that considering local failure is more rational and complete for multi-stage slopes.
2) The multi-stage slope with a smaller slope angle in the lower stage and a larger slope angle in the upper stage is more possibly subject to local failure. Large step width is of benefit to slope stability, whereas a small ratio of B/H would result in local failure of a multi-stage slope.
3) The modified pseudo-dynamic method could account for seismic effects concerning time and space. The seismic acceleration amplitude would be significantly magnified as the natural frequency of soils draw near to that of seismic waves. The damping effects of soils can reduce the adverse impacts of seismic actions. Specifically, the increase of acceleration coefficient and damping ratio would reduce the slope stability. The PDE depicts a nonlinear trend of seismic acceleration with the variation of wave velocity and vibration period, resulting in the synchronize nonlinear changes of safety factors.

DATA AVAILABILITY STATEMENT

The original contributions presented in the study are included in the article/**Supplementary Material**, further inquiries can be directed to the corresponding author.

AUTHOR CONTRIBUTIONS

Writing and Analysis: HW; Supervision: MS; Review and Editing: JW.

SUPPLEMENTARY MATERIAL

The Supplementary Material for this article can be found online at: https://www.frontiersin.org/articles/10.3389/feart.2022.798791/full#supplementary-material

REFERENCES

Baker, R., Shukha, R., Operstein, V., and Frydman, S. (2006). Stability Charts for Pseudo-static Slope Stability Analysis. *Soil Dyn. Earthq. Eng.* 26 (9), 813–823. doi:10.1016/j.soildyn.2006.01.023

Bellezza, I. (2015). Seismic Active Earth Pressure on Walls Using a New Pseudo-dynamic Approach. *Geotech. Geol. Eng.* 33 (4), 795–812. doi:10.1007/s10706-015-9860-1

Bıshop, A. W. (1954). The Use of the Slip Circle in the Stability Analysis of Earth Slopes. *Geotechnique* 5, 7–17.

Chen, G.-H., Zou, J.-F., Pan, Q.-J., Qian, Z.-H., and Shi, H.-Y. (2020). Earthquake-induced Slope Displacements in Heterogeneous Soils with Tensile Strength Cut-Off. *Comput. Geotechnics* 124, 103637. doi:10.1016/j.compgeo.2020.103637

Chen, W. F. (1975). *Limit Analysis and Soil Plasticity*. Amsterdam: Elsevier.

Chen, W. F., and Liu, X. L. (1990). *Limit Analysis in Soil Mechanics*. Amsterdam: Elsevier.

Choudhury, D., and Katdare, A. D. (2013). New Approach to Determine Seismic Passive Resistance on Retaining Walls Considering Seismic Waves. *Int. J. Geomech.* 13 (6), 852–860. doi:10.1061/(asce)gm.1943-5622.0000285

Choudhury, D., and Nimbalkar, S. S. (2006). Pseudo-dynamic Approach of Seismic Active Earth Pressure behind Retaining Wall. *Geotech. Geol. Eng.* 24 (5), 1103–1113. doi:10.1007/s10706-005-1134-x

Gao, Y.-f., Ye, M., and Zhang, F. (2015). Three-dimensional Analysis of Slopes Reinforced with Piles. *J. Cent. South Univ.* 22 (6), 2322–2327. doi:10.1007/s11771-015-2757-6

Ghosh, P. (2008). Seismic Active Earth Pressure behind a Nonvertical Retaining Wall Using Pseudo-dynamic Analysis. *Can. Geotech. J.* 45 (1), 117–123. doi:10.1139/t07-071

Griffiths, D. V., and Marquez, R. M. (2007). Three-dimensional Slope Stability Analysis by Elasto-Plastic Finite Elements. *Géotechnique* 57 (6), 537–546. doi:10.1680/geot.2007.57.6.537

He, Y., Liu, Y., Zhang, Y., and Yuan, R. (2019). Stability Assessment of Three-Dimensional Slopes with Cracks. *Eng. Geol.* 252, 136–144. doi:10.1016/j.enggeo.2019.03.001

Kramer, S. L. (1996). *Geotechnical Earthquake Engineering*. Upper Saddle River, NJ: Prentice-Hall.

Li, T. Z., and Yang, X. L. (2020a). Stability of Plane Strain Tunnel Headings in Soils with Tensile Strength Cut-Off. *Tunn. Undergr. Space Technol.* 95, 103138. doi:10.1016/j.tust.2019.103138

Li, Z.-W., Yang, X.-L., and Li, T.-Z. (2020b). Static and Seismic Stability Assessment of 3D Slopes with Cracks. *Eng. Geol.* 265, 105450. doi:10.1016/j.enggeo.2019.105450

Michalowski, R. L., and Drescher, A. (2009). Three-dimensional Stability of Slopes and Excavations. *Géotechnique* 59 (10), 839–850. doi:10.1680/geot.8.p.136

Michalowski, R. L. (2013). Stability Assessment of Slopes with Cracks Using Limit Analysis. *Can. Geotech. J.* 50 (10), 1011–1021. doi:10.1139/cgj-2012-0448

Morgenstern, N. R., and Price, V. E. (1965). The Analysis of the Stability of General Slip Surfaces. *Géotechnique* 15 (1), 79–93. doi:10.1680/geot.1965.15.1.79

Nadukuru, S. S., and Michalowski, R. L. (2013). Three-dimensional Displacement Analysis of Slopes Subjected to Seismic Loads. *Can. Geotech. J.* 50 (6), 650–661. doi:10.1139/cgj-2012-0223

Pain, A., Choudhury, D., and Bhattacharyya, S. K. (2017). Seismic Rotational Stability of Gravity Retaining Walls by Modified Pseudo-dynamic Method. *Soil Dyn. Earthq. Eng.* 94, 244–253. doi:10.1016/j.soildyn.2017.01.016

Pan, Q., Jiang, Y.-J., and Dias, D. (2017). Probabilistic Stability Analysis of a Three-Dimensional Rock Slope Characterized by the Hoek-Brown Failure Criterion. *J. Comput. Civ. Eng.* 31 (5), 04017046. doi:10.1061/(asce)cp.1943-5487.0000692

Qin, C.-B., and Chian, S. C. (2018). Kinematic Analysis of Seismic Slope Stability with a Discretisation Technique and Pseudo-dynamic Approach: a New Perspective. *Géotechnique* 68 (6), 492–503. doi:10.1680/jgeot.16.p.200

Qin, C., and Chian, S. C. (2020). Pseudo-dynamic Lateral Earth Pressures on Rigid Walls with Varying Cohesive-Frictional Backfill. *Comput. Geotechnics* 119, 103289. doi:10.1016/j.compgeo.2019.103289

Qin, C., and Chian, S. C. (2019). Pseudo-static/dynamic Solutions of Required Reinforcement Force for Steep Slopes Using Discretization-Based Kinematic Analysis. *J. Rock Mech. Geotechnical Eng.* 11 (2), 289–299. doi:10.1016/j.jrmge.2018.10.002

Shen, J., and Karakus, M. (2014). Three-dimensional Numerical Analysis for Rock Slope Stability Using Shear Strength Reduction Method. *Can. Geotech. J.* 51 (2), 164–172. doi:10.1139/cgj-2013-0191

Steedman, R. S., and Zeng, X. (1990). The Influence of Phase on the Calculation of Pseudo-static Earth Pressure on a Retaining Wall. *Géotechnique* 40 (1), 103–112. doi:10.1680/geot.1990.40.1.103

Terzaghi, K. (1950). *Mechanism of Landslides. Application of Geology to Engineering Practice*. Geological Society of America, 83.

Wang, H., Zhang, B., Mei, G., and Xu, N. (2020a). A Statistics-Based Discrete Element Modeling Method Coupled with the Strength Reduction Method for the Stability Analysis of Jointed Rock Slopes. *Eng. Geol.* 264, 105247. doi:10.1016/j.enggeo.2019.105247

Wang, L., Hu, W., Sun, D. A., and Li, L. (2019a). 3D Stability of Unsaturated Soil Slopes with Tension Cracks under Steady Infiltrations. *Int. J. Numer. Anal. Methods Geomech.* 43 (6), 1184–1206. doi:10.1002/nag.2889

Wang, L., Sun, D. A., and Li, L. (2019b). Three-dimensional Stability of Compound Slope Using Limit Analysis Method. *Can. Geotech. J.* 56 (1), 116–125. doi:10.1139/cgj-2017-0345

Wang, M.-Y., Liu, Y., Ding, Y.-N., and Yi, B.-L. (2020b). Probabilistic Stability Analyses of Multi-Stage Soil Slopes by Bivariate Random Fields and Finite Element Methods. *Comput. Geotechnics* 122, 103529. doi:10.1016/j.compgeo.2020.103529

Yang, X. L., and Li, Z. W. (2018). Factor of Safety of Three-Dimensional Stepped Slopes. *Int. J. Geomech.* 18 (6), 04018036. doi:10.1061/(asce)gm.1943-5622.0001154

Yang, X. L., and Long, Z. X. (2015). Seismic and Static 3D Stability of Two-Stage Rock Slope Based on Hoek–Brown Failure Criterion. *Can. Geotechnical J.* 53 (3), 551–558.

Zhang, Z.-L., and Yang, X.-L. (2021). Seismic Stability Analysis of Slopes with Cracks in Unsaturated Soils Using Pseudo-dynamic Approach. *Transp. Geotech.* 29, 100583. doi:10.1016/j.trgeo.2021.100583

Zhong, J. H., and Yang, X. L. (2021). Pseudo-dynamic Stability of Rock Slope Considering Hoek–Brown Strength Criterion. *Acta Geotech.*, 1–14.

Zhou, X. P., and Cheng, H. (2013). Analysis of Stability of Three-Dimensional Slopes Using the Rigorous Limit Equilibrium Method. *Eng. Geol.* 160, 21–33. doi:10.1016/j.enggeo.2013.03.027

Conflict of Interest: HW was employed by the company Zhejiang Provincial Seaport Investment & Operation Group Co., Ltd, and MS was employed by the company PowerChina Huadong Engineering Corporation Limited.

The remaining author declares that the research was conducted in the absence of any commercial or financial relationships that could be construed as a potential conflict of interest.